Nonintuitive Asymmetry in the Three-Body Photodissociation of CH_3COCN

Simon W. North,† Andrew J. Marr,† Alan Furlan,‡ and Gregory E. Hall*,†

Chemistry Department, Brookhaven National Laboratory, P.O. Box 5000, Upton, New York 11973-5000, and Physikalisch-Chemisches Institut der Universität Zürich, Winterthurerstrasse 190, CH-8057 Zürich, Switzerland

Received: July 15, 1997; In Final Form: September 30, 1997[⊗]

Pathways, energetics, and mechanisms of the 193 nm photodissociation of acetyl cyanide (CH_3COCN) have been investigated using high-resolution transient frequency modulation (FM) spectroscopy and photofragment translational spectroscopy. Vibrational and rotational state distributions of CN fragments measured by FM spectroscopy are in good agreement with previous work. The quantum yield of CN is found to be 0.9 ± 0.2. State-dependent translational energy distributions are nonstatistical. The laboratory-frame anisotropy of both velocity and angular momentum of CN fragments is vanishingly small, yet significant **v**·**j** correlations are observed, indicating a preference for the CN angular momentum to be perpendicular to the recoil velocity. Photofragment translational spectroscopy provided independent confirmation of kinetic energy distributions and fragmentation pathways. The combined measurements are consistent with the strong preference for primary CN elimination over CH_3 elimination, despite a large difference in C−C bond strengths. The primary acetyl radicals undergo virtually complete secondary dissociation.

I. Introduction

The ultraviolet photodissociation of moderate sized carbonyl compounds has attracted numerous experimental and theoretical investigations. Of the aliphatic ketones, acetone has been the most extensively studied and its dissociation dynamics are now well understood.[1−6] The α-bond cleavage occurs from the $^3(n,\pi^*)$ state over a barrier due to an avoided crossing with the repulsive $^3(n,\sigma^*)$ state. Careful analysis has suggested that the available energy is randomized prior to traversal of the exit barrier and that the product state translational and internal excitation is mediated by the repulsive interactions beyond the transition state. The $^3(n,\pi^*)$ state is reached via intersystem crossing from the $^1(n,\pi^*)$ state which can be accessed either directly by optical preparation or via internal conversion from a higher $^1(n,3s)$ Rydberg state.[7] For asymmetrically substituted aliphatic ketones the weaker of the two α-bonds is cleaved preferentially as a result of the relative barrier heights which correlate with the stability of the respective alkyl radical.[8,9] Upon nonalkyl substitution the situation becomes considerably more complicated. For example, in the ultraviolet dissociation of acetyl chloride only C−Cl bond cleavage is observed despite the near equivalence of the C−C and C−Cl bond strengths.[10−14] This selectivity can be understood by consideration of the adiabatic potential energy surfaces.[10,13] Cleavage of the C−Cl bond can occur adiabatically on the $^1A''$ surface which has $^1(n,\pi^*)$ character in the Franck−Condon region and evolves over a barrier into the repulsive $np(Cl)\sigma^*(Cl)$ state. Dissociation via this adiabatic pathway is very rapid, resulting in a strongly anisotropic distribution of photofragments. The C−C bond cleavage, which requires intersystem crossing, cannot efficiently compete. Similar behavior is observed in acetyl bromide[15,16] and acetyl iodide.[17] The photodissociation of acetic acid is another interesting example of nonintuitive preferential α-bond cleavage. Guest and co-workers have observed that the stronger C−OH bond cleaves with high yield.[18] The translational and internal energy distributions of the OH fragments indicate that the dissociation proceeds over an exit channel barrier although correlation arguments suggest that the mechanism for OH elimination is different than for CH_3 elimination. A definitive explanation for the bond cleavage preference is still outstanding.

Acetyl cyanide, CH_3COCN, which possesses an unsaturated α-substituent, represents another potentially intriguing photochemical system. Surprisingly, the photochemistry of acetyl cyanide had not been investigated until very recently.[19] The ultraviolet absorption spectrum of acetyl cyanide, shown in Figure 1, consists of two main features. The band centered at 305 nm, exhibiting coarse vibronic structure, corresponds to an excitation to the $^1(n,\pi^*)$ state. The stronger band with an onset near 230 nm is thought to involve a transition to the $^1(n,3s)$ state by analogy with other carbonyl compounds.

Recent studies have probed the nascent CN fragments arising from acetyl cyanide dissociation at 193 nm using $B\ ^2\Sigma^+ - X\ ^2\Sigma^+$ laser-induced fluorescence (LIF) and established the energetics of the possible fragmentation pathways using ab initio calculations.[19,20] At 193 nm excitation (619 kJ mol^{-1}), cleavage of either the C−CN or C−CH_3 bond can occur,

$$CH_3COCN \rightarrow CH_3CO(X\ ^2A') + CN(X\ ^2\Sigma^+) \qquad \Delta H^0 = 427 \text{ kJ mol}^{-1} \quad (1)$$

$$CH_3COCN \rightarrow CH_3(X\ ^2A_2'') + OCCN(X\ ^2A') \qquad \Delta H^0 = 359 \text{ kJ mol}^{-1} \quad (2)$$

The relative strength of the C−CN bond reflects the effect of partial conjugation with the carbonyl moiety which also results in a contraction of the bond length.[19] If sufficient energy of the initial bond cleavage is partitioned into the photofragment internal degrees of freedom, the secondary dissociation of either OCCN

$$OCCN \rightarrow CO + CN \qquad \Delta H^0 = 126 \text{ kJ mol}^{-1} \quad (3)$$

or CH_3CO

$$CH_3CO \rightarrow CH_3 + CO \qquad \Delta H^0 = 48 \text{ kJ mol}^{-1} \quad (4)$$

is the end result. Figure 2 shows a schematic energy level

* Corresponding author. Email: greghall@bnl.gov.
† Brookhaven National Laboratory.
‡ Universität Zürich.
⊗ Abstract published in *Advance ACS Abstracts,* November 15, 1997.

S1089-5639(97)02293-7 CCC: $14.00

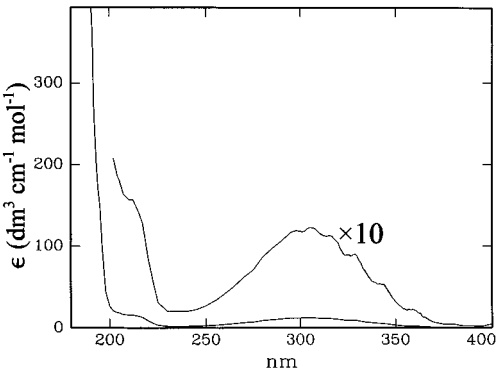

Figure 1. Ultraviolet absorption spectrum of gas-phase acetyl cyanide recorded on a Cary 210 spectrophotometer.

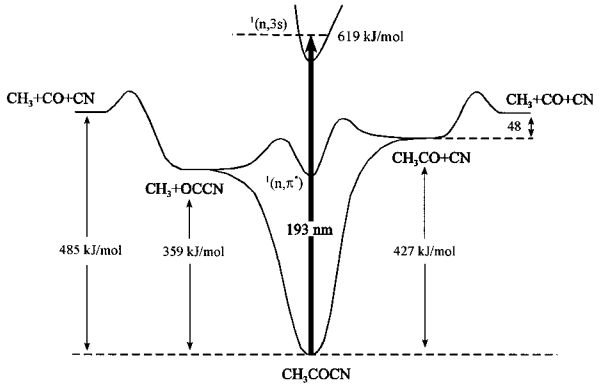

Figure 2. Schematic energy diagram for acetyl cyanide dissociation at 193 nm. The energetics are taken from refs 19 and 20.

diagram for the dissociation of acetyl cyanide. Horwitz *et al.*[19] determined that the nascent CN rotational and vibrational distributions could be well described by a Boltzmann temperature of 1800 K. Analysis of the Doppler-broadened excitation lines were consistent with a translational temperature of 2600 ± 800 K. From energetic considerations these authors[19] concluded that the observed CN originated from reaction 1 alone, rather than the sequence of reactions 2 and 3.

In the present paper, we report scalar and vector properties of the CN fragments arising from the 193 nm dissociation of acetyl cyanide. Nascent CN Doppler profiles were measured using high-resolution frequency-modulation (FM) spectroscopy. Some advantages of this technique, which include sensitivity near the shot-noise limit and line widths characteristic of single-mode cw lasers, have been previously demonstrated.[21,22] We have also performed photofragment translational spectroscopy (PTS) experiments to search for all the dissociation products. This technique provides a broad overview of the dissociation and complements the state-specific measurements on CN. These new measurements generally confirm and extend the earlier work on this system, providing further insight into the nature of the dissociation dynamics. We concur with Horwitz *et al.*[19] that most of the CN comes from the primary dissociation of CH_3COCN. Further, we present evidence that this is the only significant primary channel and that almost all of the coincident CH_3CO has too much internal energy to survive.

II. Experimental Section

A. Transient FM Measurements. The general features of the transient FM experimental apparatus have been described in detail elsewhere.[23,24] Briefly, the 193 nm photolysis light was furnished by the unfocused beam from an ArF excimer laser operating at 12 Hz. This unpolarized photolysis beam was passed through 10 fused silica plates at Brewster's angle with respect to the direction of propagation resulting in >95% linear polarization. Each pulse provided fluences of 5−20 mJ/cm^2 to the sample. For the absorption cross section measurements the photolysis laser power was detected with a pyroelectric energy meter (Molectron J50) with 100 shot averaging on a digital oscilloscope.

The nascent ($X\ ^2\Sigma^+$) CN radical photoproducts were probed in the $\Delta v = 2$ bands of the $A\ ^2\Pi \leftarrow X\ ^2\Sigma^+$ system near 800 nm using continuous radiation from a Ti:sapphire ring laser. The cw probe beam was frequency modulated at 200 MHz, overlapped with the photolysis beam, and imaged onto a fast photodiode. The 3−4 mm diameter probe beam was maintained below 35 mW to avoid saturation of the optical transitions. The 200 MHz beat signal resulting from the differential absorption or retardation of the two sidebands by the CN photofragments was high-pass filtered, amplified, and measured by an I&Q demodulator. The transient signals were averaged in a digital oscilloscope over multiple excimer laser shots and archived in a lab computer at a sequence of laser frequencies across selected CN rotational lines. The measurements consist of a two-dimensional array of signal vs time and laser frequency, from which the time-dependent line shapes and intensities can be selected for subsequent analysis.

Measurements were performed in a 1.5 m single-pass collinear cell in which the probe and photolysis beams copropagate and in a transverse multipass cell in which the frequency-modulated probe laser beam made multiple traversals between plane-parallel dielectric mirrors aligned parallel to the photolysis laser propagation direction.[25] In both arrangements a slow flow (4 sccm) of acetyl cyanide was maintained at total pressure of <20 mTorr for nascent data. Acetyl cyanide (Aldrich) was subjected to several freeze−pump−thaw cycles prior to use. Similar flow and pressure conditions were used for acetone and cyanogen measurements employed in determining the 193 nm acetyl cyanide absorption cross section and CN quantum yield. The transverse cell arrangement was also used for double-magic-angle measurements (see section IIIB). In those particular experiments a Soleil-Babinet compensator (Special Optics) and an air-spaced calcite Glan prism were used to produce the required polarization state of the probe laser beam.

Nascent data were acquired with 100 shot averaging at each 100 MHz frequency step, selecting data from the first 100 ns following photolysis. Inspection of the time dependence of the Doppler profiles indicated that negligible translational or rotational relaxation had occurred in this time. Thermalized lines were obtained by increasing the total pressure with Ar and selecting the FM spectra 5 μs after the photolysis pulse. Procedures for reconstructing the Doppler profiles from the two-channel FM line shapes have been previously described.[24]

B. Photofragment Translational Spectroscopy Measurements. The photofragment translational spectroscopy (PTS) experiments were performed at the University of Zürich in a spectrometer which has been described in detail elsewhere.[26] It consists of a rotatable, pulsed molecular beam source, a 34.5 cm long drift tube, an electron bombardment ionizer, a quadrupole mass spectrometer for mass filtering, and an electron multiplier for detection. Samples of 7% acetyl cyanide in He were introduced at a stagnation pressure of 300 Torr through a piezoelectric valve with an exit attachment heated to 90 °C to minimize the contribution from clusters. Unpolarized photolysis light at 193 nm was weakly focused to a fluence of about 400 mJ/cm^2 in the interaction region 5 cm from the pulsed source. A few measurements were made with polarized photolysis light to assess the velocity anisotropy. The combination of a Brewster angle stack of fused silica plates and a half-wave plate reduced

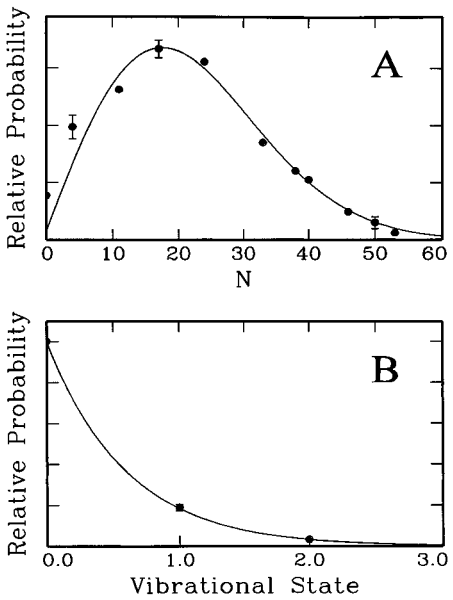

Figure 3. (A) Rotational state distribution for nascent CN($X^2\Sigma^+$) fragments in $v = 0$ from the 193 nm photodissociation of acetyl cyanide. The solid line represents a 1800 K Boltzmann fit to the experimental data. (B) Nascent vibrational distribution for CN fragments from the 193 nm photodissociation of acetyl cyanide. The solid line represents the best-fit Boltzmann distribution with a temperature of 1750 K.

the fluence by a factor of about four. The velocity distribution of the molecular beam source was determined using a chopper wheel synchronized with the pulsed valve. Forward convolution analysis[27] of the mass-resolved time-of-flight (TOF) signals was used to derive total center-of-mass kinetic energy distributions for the detected fragments.

III. Results

A. State Distributions. We have measured the relative populations of selected rotational states of CN ($v = 0$) from the areas under phase corrected and transformed nascent Doppler profiles using R_1 transitions.[24] The populations, normalized for photolysis and probe power, are shown as the solid circles in Figure 3A. The rotational quantum number N denotes the total angular momentum of CN excluding spin. The solid line in Figure 3A is a Boltzmann distribution with a rotational temperature of 1800 K, which was used to describe the rotational state distribution measured by Horwitz *et al.*[19] using B−X LIF. Our measurements are in exact agreement. Although we do not report CN rotational distributions for $v = 1$ and $v = 2$, the relative intensities of nascent Doppler profiles in those vibrational states were also consistent with the rotational distributions of Horwitz *et al.*[19]

The intensities of rotationally and translationally thermalized absorption lines can be compared to determine nascent vibrational populations.[21,22] The measured signal intensities are given by

$$I(v,N) \propto q_{v''v} S_{J''J'} \exp(-E_{rot}/kT) P(v) \qquad (5)$$

where $q_{v'v''}$ is the ($A^2\Pi-X^2\Sigma^+$) Franck−Condon factor,[28] $S_{J''J}$ is the rotational line strength factor,[29] and $P(v)$ is the probability of forming fragments in a particular vibrational state. The ratios of integrated areas of transitions in different vibrational bands, after correcting for both the photolysis and probe power, yields the ratio of product vibrational states through eq 5. In order to determine the $v = 2{:}1{:}0$ branching ratios, we compared thermalized $R_1(15.5)$ transitions of the (4−2), (3−1), and (2−0) vibrational bands. Separate comparisons of $v = 0{:}1$ and $v = 1{:}2$ were made at different pressures of acetyl cyanide to expand the dynamic range of the measurements. A $v = 1{:}0$ vibrational ratio of 0.190 ± 0.015, and a $v = 2{:}1$ vibrational branching ratio of 0.181 ± 0.030 were obtained, where the stated error reflects 1 σ from multiple scans. Combining these measurements produces a final experimental vibrational distribution of 0.82:0.15:0.03 for $v = 0{:}1{:}2$, shown as the solid circles in Figure 3B. The solid line is the best-fit Boltzmann vibrational distribution and corresponds to a temperature of 1750 K, in good agreement with the CN vibrational distribution reported by Horwitz *et al.*[19]

B. CN Doppler Analysis. Procedures for analyzing Doppler-broadened profiles which arise from linearly polarized single-photon photolysis and detection have been reported previously.[25,30,31] Here we describe our favored procedure for extracting center-of-mass speed distributions and average vector correlations, in the case of broadly distributed velocity distributions.

In single-photon detection schemes there exists a "double magic angle" excitation-detection geometry, at which only the speed distribution and the **v·j** correlation parameter, $\beta_0^0(22)$, influence the Doppler profile. This geometry is obtained for a probe beam propagating at 54.7° from the dissociation polarization axis, and polarized 45° from the plane defined by the dissociation polarization axis and the probe propagation direction. In this geometry, the laboratory frame Doppler profile is given by

$$D'(w) = \int_{|w|}^{\infty} (1/2v)[1 - h^{(2)}\beta_0^0(22)' P_2(w/v)] v^2 f'(v)\, dv \qquad (6)$$

The primes refer to laboratory frame quantities, w is the Doppler shift in velocity units, $v^2 f'(v)$ is the laboratory speed distribution, P_2 is the second Legendre polynomial, $h^{(2)}$ depends only on the rotational branch, having the value $h^{(2)} = -1$ for absorption on a Q-branch line, and $h^{(2)} = J/(2J + 3)$ for absorption on an R-branch line, and the lab frame bipolar moment describing the **v·j** correlation, $\beta_0^0(22)'$, is in general a function of velocity, v. A pair of Q- and R-branch Doppler profiles measured at the double magic angle, normalized to unit area and added with a Q:R weighting of $1{:}(2 + 3/J)$ cancels the remaining laboratory correlation, $\beta_0^0(22)'$, giving an isotropic composite Doppler profile, $D'_0(w)$.

$$D'_0(w) = {}^1/_2 \int_{|w|}^{\infty} v f'(v)\, dv \qquad (7)$$

This (and, indeed, any) laboratory-frame Doppler profile is a one-dimensional convolution of the center-of-mass Doppler profile, $D(w)$, with the parent thermal velocity distribution along the Doppler probe direction,

$$D'(w) = \left(\frac{M}{2\pi kT}\right)^{3/2} \int_{-\infty}^{\infty} D(w-v) e^{-Mv^2/2kT}\, dv \qquad (8)$$

where M is the parent mass and T the temperature. An advantage of the continuous laser probe used in the present Doppler measurements is that no significant additional broadening is caused by the laser line width, so the convolution relating the center-of-mass and laboratory frames depends on no unknown parameters or functional forms.

Equations 7 and 8 imply that the center-of-mass speed distribution can be obtained formally from the composite Doppler profile by deconvolution followed by differentiation. However, deconvolution of the original laboratory-frame signal, $D'_0(w)$, by a Gaussian function is a highly unstable transformation, equivalent to applying a frequency domain filter with unit

gain at low frequencies, and exponentially increasing gain with the squared frequency. Deconvolution of experimental data typically requires aggressive low-pass filtering to avoid catastrophic instability. Fitting to a truncated set of Gaussian-weighted polynomials is one means of filtering the experimental data enough to allow deconvolution.[32,33] We have returned to older and simpler style of Doppler analysis[34,35,36] using an adjustable center-of-mass translational energy distribution in a forward convolution fitting procedure. Rather than a Gaussian distribution of translational energies, we have chosen the following functional form

$$P(E_T) = [E_{avail} - E_{CN}(v,N)][f_T^a(1 - f_T)^b] \qquad (9)$$

where f_T is the fraction of the available energy in translation, E_{avail} is the total available energy, $E_{CN}(v,N)$ is the internal energy of the detected CN state, and a and b are adjustable parameters. This particular functional form of the translational energy distribution is appealing because it is a flexible two-parameter function which is positive definite, conserves the total available energy, and contains no higher frequency components than are required by the conservation laws. A sharp cutoff in intensity at a maximum velocity is difficult to represent in a truncated expansion of polynomials, yet appears naturally in the form of eq 9. Complex, multicomponent systems cannot be well described, but broad distributions extending up to (but not beyond) a maximum kinetic energy can be well represented. An initial trial translational energy distribution is transformed to a CN center-of-mass speed distribution and used to generate a center-of-mass Doppler profile. The Doppler profile is convolved with the parent velocity distribution according to eq 8 and compared to the experimental composite Doppler profile. The least-squares optimum values of parameters a and b are found by a simplex search.[37]

Once the center-of-mass speed distribution, $u^2f(u)$, has been determined from the double magic angle measurements, Doppler profiles recorded in different excitation-detection geometries are then fit with one additional parameter, a velocity-averaged, center-of-mass β_{eff}. Simulated Doppler profiles are calculated using eq 10, followed by convolution with the parent molecular velocity distribution.

$$D(w) = \int_{|w|}^{\infty} \frac{1}{2u}[1 + \beta_{eff}P_2(w/u)]u^2f(u)\,du \qquad (10)$$

The set of β_{eff} parameters for different rotational branches and experimental geometries are combined by standard methods[25,31,38] to yield a set of bipolar moments, characterizing the vector correlations among the parent transition moment, the fragment angular momentum, and the fragment recoil velocity. From such analysis we find that of the measurable center-of-mass bipolar moments, none except $\beta_0^0(22)$ has an absolute magnitude greater than 0.01. Specifically, neither the velocity nor the fragment angular momentum is detectably aligned in the lab frame.

In the absence of laboratory-frame alignment, the Doppler profiles measured in *any* experimental geometry, not just the double magic angle, depend only on the **v·j** correlation and the speed distribution according to eq 6. For the most accurate determination of speed distributions and **v·j** correlations, we therefore used Doppler profiles collected in the collinear geometry, where superior signals could be obtained. The simultaneous fitting of the Q- and R-branch data provides a center-of-mass speed distribution and a center-of-mass **v·j** correlation, by the same method described above for the double magic angle measurements. Figure 4 shows a selection of

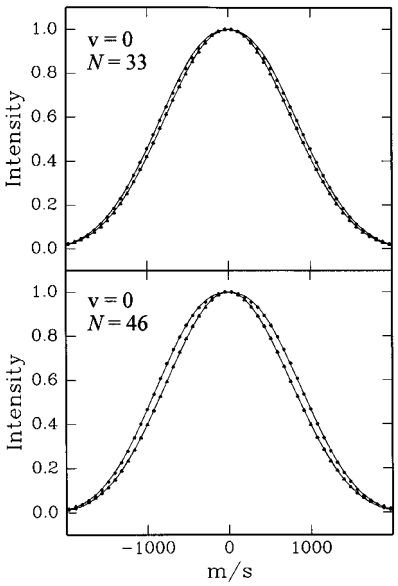

Figure 4. Nascent Doppler profiles for selected CN($X\ ^2\Sigma^+$) Q- and R-branch lines in $v = 0$. Experimental data are shown as symbols for the Q-branch (broader) and R-branch (narrower) measurements. The solid lines are single-parameter fits to the data using eq 6.

TABLE 1: Center-of-Mass Velocity-Averaged CN v·j Correlations $\langle\beta_0^0(22)_v\rangle$ and Average Total Translational Energies $\langle E_T\rangle$ from CH_3COCN Photodissociation at 193 nm

	N	$\langle\beta_0^0(22)_v\rangle$	$\langle E_T\rangle$ (kJ/mol)
$v = 0$	11	-0.035 ± 0.03	30.4 ± 0.7
	17	-0.04 ± 0.03	30.3 ± 0.7
	24	-0.055 ± 0.02	30.4 ± 0.7
	30	-0.07 ± 0.02	30.1 ± 0.7
	33	-0.06 ± 0.02	30.5 ± 0.7
	38	-0.10 ± 0.02	31.2 ± 0.7
	46	-0.13 ± 0.03	29.1 ± 0.9
	50	-0.16 ± 0.04	29.4 ± 1.0
	53	-0.23 ± 0.05	25.8 ± 1.5
$v = 1$	16	-0.01 ± 0.02	29.8 ± 1.0
	21	-0.02 ± 0.02	29.2 ± 1.0
	28	-0.08 ± 0.02	28.1 ± 1.5
	36	-0.16 ± 0.03	24.1 ± 1.5
$v = 2$	12	-0.055 ± 0.03	24.6 ± 3.0
	16	-0.10 ± 0.04	24.5 ± 3.0
	22	-0.13 ± 0.05	27.8 ± 3.0

nascent Q- and R-branch Doppler profiles for representative CN-(v,N) states with the forward-convolution fits. The state-dependent values of the **v·j** correlations are summarized in Table 1 and plotted in Figure 5.

The center-of-mass speed distributions also provide valuable information regarding scalar correlations in the dissociation. The forward convolution fits to two representative $D'_0(w)$ composite Doppler profiles are shown as solid lines in Figure 6, A and C. The solid circles are the experimental data. The dashed line in Figure 6A represents the contribution of the initial parent motion to the laboratory-frame Doppler profiles. The CN translational energy distributions used to fit these Doppler profiles are expressed as a total translational energy, assuming CH_3CO as the cofragment, and plotted in Figure 6, B and D. Average values are given in Table 1 for each measured CN state. The average translational energy of the CN fragment alone is about 19 kJ/mol for fragments in $v = 0$, and decreases only slightly with CN vibrational quantum number. Horwitz *et al.*[19] reported substantially higher average CN translational energies, based on Doppler profile measurements near the resolution limits of their pulsed dye laser. They found that a satisfactory fit to selected Doppler profiles could be achieved using a Boltzmann velocity distribution for the CN fragments with a temperature

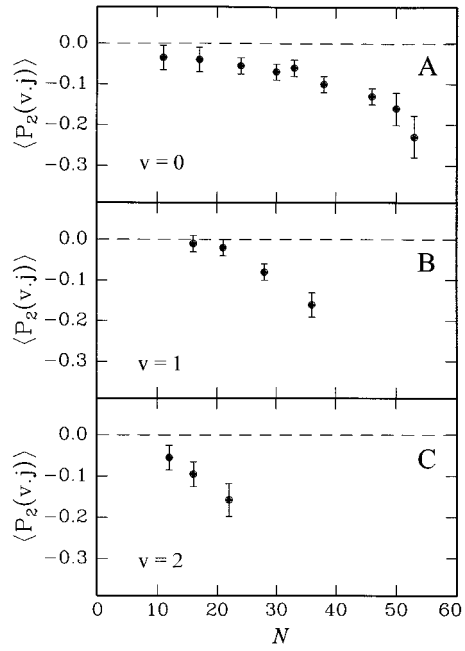

Figure 5. Measured **v·j** correlations as a function of N for selected CN states in (A) $v = 0$, (B) $v = 1$, and (C) $v = 2$.

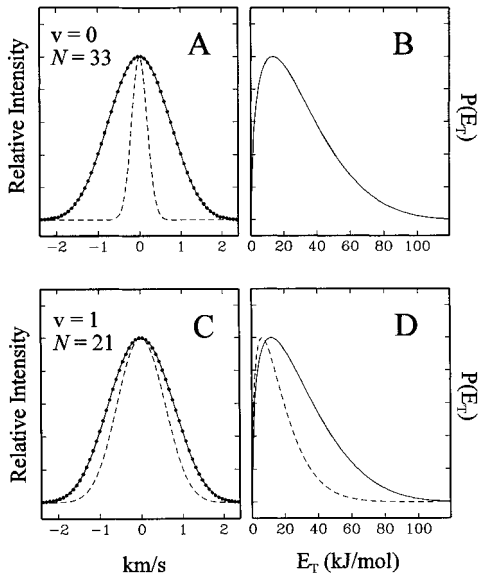

Figure 6. Closed circles show isotropic composite Doppler profiles for CN($X\ ^2\Sigma^+$) fragments in (A) $v = 0$, $N = 33$ and (C) $v = 1$, $N = 21$. The solid lines are the best-fit to the data using the forward convolution model described in the text. The 300 K acetyl cyanide parent Doppler profile is shown as the dashed line in (A). Total translational energy distributions corresponding to the forward convolution fits are shown in (B) and (D). Shown as the dashed lines in (C) and (D) are the prior model predictions for the CN Doppler profile and total translational energy distribution, respectively.

of 2600 ± 800 K which corresponds to a mean translational energy of 32 ± 10 kJ/mol. Our average values are slightly below this lower error bound.

C. CN Quantum Yield. Doppler line shape measurements are only sensitive to scalar and vector properties of the CN fragments. Complementary measurements of the CN quantum yield can provide vital information regarding the identity of the other fragments and the mechanism of dissociation. In order to determine the absolute CN quantum yield from acetyl cyanide, Φ_{CN}, it is necessary to first establish a value for the absorption cross section. The effective absorption cross section at 193 nm depends on the spectral overlap of the structured ArF emission and the steeply sloped absorption profile. Consequently, rather than obtaining a value from the absorption profile shown in Figure 1, we determined the effective cross section by measuring the attenuation of the 193 nm photolysis light through our single-pass absorption cell at various pressures of acetyl cyanide. From a series of such measurements we have obtained a value of $(1.2 \pm 0.2) \times 10^{-18}$ cm^2 for the 193 nm absorption cross section. To check our procedure, the cross section of acetone at 193 nm was determined by a similar procedure and compared to its recently reported value.[39] Our result for acetone was in good agreement with that previous measurement; the error apportioned to the acetyl cyanide cross section reflects the small difference in the values observed.

The absolute CN quantum yield was determined by comparing CN signal intensities from acetyl cyanide with cyanogen at 193 nm. Cyanogen (NCCN) is a convenient reference molecule since the CN quantum yield, product state distributions, and absorption cross section are well-known.[22,40] To simplify the analysis, the CN intensities were compared following rotational and translational thermalization, but before significant vibrational relaxation or reaction had occurred. CN signals for both acetyl cyanide and cyanogen from the $R_1(15.5)$ line of the (2−0) band were measured. The 193 nm absorption cross section of NCCN is 2.0×10^{-19} cm^2 and the fractional population of nascent CN in $v = 0$ is 0.87. Using these values and assuming a CN quantum yield of 2.0 for NCCN, we calculate a CN quantum yield of 0.9 ± 0.2 from acetyl cyanide photodissociation at 193 nm.

D. Photofragment Translational Spectroscopy. Photofragment translational measurements were made at $m/e = 15$ (CH_3^+), 26 (CN^+), 27 (HCN^+), 28 (CO^+), 42 (CH_2CO^+), 43 (CH_3CO^+), and 54 ($OCCN^+$). Extensive averaging resulted in no detectable photofragment signals at the CH_3CO^+ or $OCCN^+$ masses. There were also no detectable photofragment signals at the HCN^+ or CH_2CO^+ masses. HCN and CH_2CO are the products analogous to those calculated to be formed in the lowest barrier dissociation process from the ground state of acetyl chloride.[13] The background at $m/e = 28$ was too high to measure useful signals for the CO^+ mass. CN^+ signals at $m/e = 26$ were measured at source angles of 30°, 18°, and 9°. The time-of-flight (corrected for ion flight time) at 9° is shown in Figure 7A, along with a forward convolution fit to the kinetic energy distribution, assuming CN to be a primary photoproduct. The corresponding $P(E_T)$ is shown in Figure 7B, which is in good agreement with the total center-of-mass kinetic energy distributions in Figure 6, derived from the CN Doppler spectroscopy. The photolysis laser polarization dependence of the CN^+ signal was measured, and showed no sign of anisotropy, consistent with the Doppler FM measurements. The similarity of the CN fragment $P(E_T)$ derived from the FM Doppler and the PTS measurements gives some confidence that multiple photon excitation and secondary excitation of primary photoproducts are not important in these PTS measurements, despite the relatively high laser fluences used. Apart from a reduction in signal levels, the $m/e = 26$ TOF signals observed with reduced power in the polarized photolysis experiments showed no signs of multiphoton effects or secondary photolysis. The absence of CH_3CO^+ signal is consistent with an essentially complete secondary fragmentation of CH_3CO.

The $m/e = 15$ signals were also collected at 30°, 18°, and 9°. Trial fits to these signals were attempted, assuming primary production of CH_3 + OCCN (reaction 2). An energy distribution with an average kinetic energy of about 50 kJ/mol can describe the CH_3^+ signal, not dissimilar to the primary methyl elimination from acetone at 193 nm.[1] The average energy left

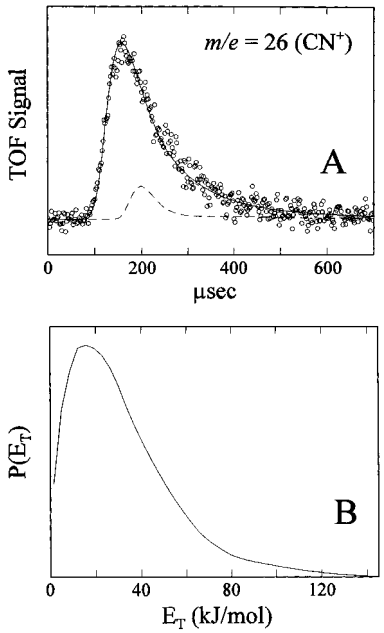

Figure 7. (A) Photofragment translational spectrum of CN^+ measured at 9° from the molecular beam (points). The solid line is a forward convolution fit using the primary $P(E_T)$ for fragmentation to CN + CH_3CO shown in panel B. The dashed line is the (missing) contribution that might be expected from dissociative ionization of OCCN if the CH_3+ signal is attributed to a primary photofragment. (B) Total translational energy distribution used to fit the CN^+ signals at three laboratory angles.

for total internal energy of primary CH_3 and OCCN would then be 210 kJ/mol. If about half of this energy is partitioned into each four-atomic fragment, a substantial fraction of primary OCCN should have insufficient energy to break the 126 kJ/mol C−C bond,[19] and even more would be unable to surmount the unknown barrier above this. We were, however, unable to detect any trace of stable OCCN at the low background mass of 54, an argument against reaction 2 as the dominant source of CH_3 fragments. The TOF signals for mass 26 can also be inspected for evidence of a possible contribution due to dissociative ionization of OCCN to give CN^+. This would be a possible explanation for our failure to observe stable OCCN radicals if they were there. A stable OCCN radical, momentum matched to the CH_3 (assuming it to be a primary fragment), could contribute to the CN^+ signal at the times marked by the dashed peak in Figure 7A. The kinematics would be favorable for detecting this slow fragment, which would appear as a sharp feature superimposed on the broad CN^+ TOF signal. If primary methyl elimination contributed 10% of the total dissociation (the balance assumed to be primary CN elimination) and half of the COCN underwent dissociative ionization to CN^+, a detectable sharp feature would contribute to the total CN TOF signal with a relative intensity as illustrated by the dashed line shown in Figure 7A. No sign of such a contribution to the mass 26 signal was observed at any angle. In subsequent measurements,[41] we have succeeded in detecting substantial $OCCN^+$ signal from the 193 nm photodissociation of $(CN)_2CO$, proving that this radical is stable and survives electron impact ionization, strengthening the PTS evidence against significant amounts of the primary CH_3 + OCCN channel in this photodissociation.

An alternative fit to the CH_3 signals was performed, assuming the secondary dissociation of CH_3CO (reaction 4) to be the dominant source of CH_3. The primary $P(E_T)$ was fixed from the CN analysis, along with a secondary angular and kinetic energy distribution similar to those used to fit secondary acetyl dissociation in previous studies.[1] While the CH_3 data are too noisy to justify a true fit, they are not inconsistent with the energetics and kinematics of the secondary dissociation of highly excited CH_3CO.

IV. Discussion

A. Origin of the Observed CN. Despite the near unity CN quantum yield determined in the previous section, we need to discriminate between the two possible origins of the CN fragments. The information obtained from the Doppler line shape analysis and PTS experiments, when compared with various models of dissociation, provides compelling evidence in favor of a primary fragmentation mechanism for the production of CN.

The 619 kJ/mol of excitation energy is sufficient to cleave either α-bond. On the basis of the relative bond dissociation energies one would expect CH_3 to be produced preferentially to CN.[42] In this case the majority of the detected CN would originate from a two-step fragmentation (reactions 2 and 3). The probability of this fragmentation pathway has been examined by Horwitz *et al.*[19] The authors assumed a 56 kJ/mol exit barrier in CH_3 + OCCN fragmentation which evolves exclusively into product translation and that the OCCN fragment persists for several rotational periods prior to undergoing secondary dissociation. The measured average CN fragment translational energy can be scaled according to this model to give the total translational energy of all three fragments. The result was an unreasonably large fraction of the total available energy of 134 kJ/mol, leaving too little for internal energy of the fragments. The authors[19] therefore reject the primary CH_3 elimination mechanism.

A similar argument using the present state-dependent CN translational energy distributions up to $v = 2$ can provide stronger evidence that CN is produced from primary dissociation. For high rotational states ($N > 50$) in $v = 0$ and moderate rotational states in $v = 1$ and $v = 2$, the two-step treatment outlined above results in total translational energies which exceed the available energy. These most highly excited CN fragments thus cannot originate from the secondary dissociation of OCCN. The Doppler profiles measured for these states are nearly indistinguishable from the full set of experimental $v = 0$ Doppler profiles, suggesting that the lower energy CN fragments are similarly produced from reaction 1.

An alternative procedure for establishing the origin of the CN fragments involves comparing the CN quantum yield predicted by simple dissociation models with our experimental value. Based solely on the energetics of the C−CH_3 bond cleavage channel, it is possible to estimate the internal excitation of the OCCN fragment. A statistical partitioning of the available energy, used to describe dissociation on a barrierless ground-state potential energy surface, provides an upper limit to the fragment internal excitation and can be approximated by the prior model.[43] The average OCCN internal energy predicted by this model is 118 kJ/mol, less than the 126 kJ/mol required to break the OC−CN bond. This suggests that if CH_3 elimination does occur, the majority of nascent OCCN radicals would be stable with respect to secondary fragmentation. The existence of an exit barrier to OCCN dissociation would further increase the fraction of stable OCCN. The measured CN quantum yield of 0.9 ± 0.2 is, therefore, inconsistent with a significant contribution from primary CH_3 elimination. The absence of signal at $m/e = 54$ ($OCCN^+$) in the PTS experiments is additional evidence that the dissociation proceeds via initial CN elimination.

B. Vector Correlations. The negative measured values of $\beta_0^0(22)$ indicate a preference for the CN angular momentum, **j**,

TABLE 2: Product Energy Partitioning (kJ/mol) from the 193 nm Photodissociation of CH_3COCN [$CH_3COCN \rightarrow CH_3CO + CN$]

	E_R(CN)	E_V(CN)	E_T(CN)	$E_{int}(CH_3CO)$	$E_T(CH_3CO)$
impulsive	0.0	51.8	44.4	69.4	26.9
prior	11.3	11.3 (4.0)[a]	10.6	152.9	6.4
BIM	13.0	13.6	19.0	135.1	11.5
experiment	14.9 ± 2.5	5.1 ± 0.3	19.0 ± 0.6	141.5[b]	11.5 ± 0.3

[a] The number in parentheses is the result obtained from a discrete integration of the continuous prior distribution. [b] Using $E_{avail} - \langle E_{int}(CN)\rangle - \langle E_T(total)\rangle$.

to be perpendicular to the recoil velocity, **v**. The **v·j** correlation increases for the higher energy states of CN, reaching almost half the limiting value of −0.5 for CN(v=0, N=53). Unlike the laboratory-frame alignment of **v** or **j**, which can be significantly diminished by parent rotation prior to dissociation, the **v·j** correlation is determined by the forces and torques operating at the instant of fragmentation. In slow predissociations, involving either internal conversion or intersystem crossing prior to reaction, it is the **v·j** correlation which can provide valuable insight into the nature of the potential energy surface in the region beyond the transition state. The observation of **v·j** correlations in photofragmentation has traditionally been considered to indicate nonstatistical fragmentation and until recently there was no prescription for predicting the statistical expectation of the **v·j** correlation.[44,45] It is now understood that moderate **v·j** correlations can arise solely from angular momentum conservation even in barrierless dissociation. The magnitude of such correlations is expected to be small, however, for systems with large initial parent rotation, J, which relaxes the constraints on the fragment angular momenta. In addition, the **v·j** correlation should be negligible for the fragment with the larger rotational constant.[44] As a consequence, no correlation between **v** and **j** for the CN fragment is expected by statistical theory for this system. The measured CN **v·j** correlations must, therefore, arise from dynamical factors in the dissociation.

The bias toward perpendicular **v** and **j** could be the result of several dynamical effects in the primary elimination of CN. The effect of the initial parent angular momentum on CN rotational excitation can be shown to be negligible using a simple kinematic model presented by Uberna *et al.*[46] An impulsive torque associated with a nonlinear C−C−N configuration during the C−C repulsion would generate CN angular momentum perpendicular to the recoil velocity. In a direct repulsive dissociation this would be a dominant effect, leading to a strong negative **v·j** correlation, even for the lower rotational levels. The mapping of C−C−N bending motions of the parent molecule at the transition state onto CN rotation would also contribute an excess component of **j** perpendicular to **v**, while the vibrational angular momentum of this degenerate bend will evolve into a component of **j** parallel to **v**. Exit channel effects are likely to provide an additional bias to the angular distribution of **j** based on the angular anisotropy of the potential beyond the transition state.

The observed **v·j** correlations provide good evidence against a statistical ground-state dissociation, fair evidence against a direct excited-state dissociation, and can be considered consistent with the dynamical effects of a modest exit barrier.

C. Model for the Dissociation. In light of the evidence that the dissociation occurs primarily via reaction 1, we now attempt to formulate a description of the C−CN bond cleavage process. We test the feasibility of various dissociation mechanisms by comparing our experimental results with the predictions of simple, limiting, dynamical models.

The transition to the ^{1}(n,3s) Rydberg state should be polarized in the plane of the molecule, approximately perpendicular to the CO direction, based on the local C_{2v} symmetry of the carbonyl chromophore. Prompt dissociation along a C−CN bond in the ground-state geometry would lead to an anisotropy parameter of $\beta = 1.25$. The lack of photofragment anisotropy suggests that the dissociation is not the result of prompt fragmentation and, therefore, does not involve excitation to a repulsive electronic state. An excitation polarized along the C−O bond followed by prompt dissociation along a 60° angle (close to the magic angle, 54.7°) could give nearly isotropic direct fragments, although the carbonyl chromophore should have no nearby transitions of this symmetry. Furthermore, in a prompt dissociation the kinetic energy can usually be fairly well approximated using the impulsive model, which assumes that the available energy is released as a repulsion localized in the reaction coordinate.[47] The average energies predicted by this model are given in Table 2. The model partitions a substantial fraction of the available energy into fragment recoil and severely overestimates the translational energy observed. The preference for breaking the stronger C−CN bond over the C−CH_3 bond is, therefore, not the result of a dissociation mechanism similar to that proposed for the acetyl halides,[10,15−17] where strong photofragment anisotropy is observed and the energy partitioning is fairly well described by the impulsive model.

A second mechanism, consistent with an isotropic fragment velocity distribution, involves dissociation on the ground electronic state following internal conversion. The association of two ground state radical fragments should proceed on a barrierless potential energy surface and the energy partitioning for dissociation, related by time reversal to the recombination, should be well described by statistical theory. The results from the prior model given in Table 2 reproduce the observed CN rotational and vibrational energy reasonably well. The modest deviations in the predicted vibrational energy might be expected, due to the high total energy above the reaction threshold energy, and the deficiencies of the continuous oscillator model used in the vibrational prior distribution. The measured translational energy of the fragments, however, is much greater than the prior prediction. We can directly compare the prior prediction with experimental Doppler profiles to emphasize this point. The prior translational energy distribution is given by

$$\rho^0(f_T|E) = f_T^{1/2}(1 - f_T)^{s_2+5/2} \qquad (11)$$

where f_T is the fraction of the available energy in translation and s_2 is the number of vibrational degrees of freedom in the CH_3CO radical. Figure 6C shows that the CN Doppler profile corresponding to the prior distribution is clearly unsatisfactory in describing the experimental data. There are two additional observations that suggest that the dissociation does not occur on the electronic ground state. First, as mentioned previously, the observed CN **v·j** correlations are inconsistent with a statistical partitioning of the available energy. Furthermore, a ground-state radical dissociation should favor the much less endothermic C−CH_3 channel over CN elimination. A molecular channel giving HCl and ketene has been calculated to be the

lowest barrier dissociation pathway on the ground-state potential energy surface of acetyl chloride.[13] The analogous products HCN and ketene were not detected in our acetyl cynanide PTS measurements. The strong preference for C−CN bond cleavage, the observed CN **v**·**j** correlations, and the translational energy suggest that the dissociation occurs from an electronically excited state.

In the ultraviolet photodissociation of moderate sized aliphatic carbonyl compounds, α-bond cleavage usually proceeds over an exit barrier with the majority of the potential energy beyond the barrier released as product translation. To predict the partitioning of available energy for such a dissociation it is necessary to have a model that reflects the impulsive nature of the exit barrier as well as the statistical distribution of energy in excess of the barrier height. The barrier impulsive model (BIM) is a simple model that has been successfully applied to the energy partitioning in polyatomic molecules that possess a substantial exit barrier.[1,48,49] A detailed description of the model can be found elsewhere.[1] Briefly, the available energy is divided into two "energy reservoirs"

$$E_{\text{avail}}(\text{tot}) = E^{\text{stat}}(\text{tot}) + E^{\text{imp}}(\text{tot}) \qquad (12)$$

The energy content of the impulsive reservoir, $E^{\text{imp}}(\text{tot})$, is equivalent to the exit barrier height and is partitioned according to the rigid fragment limit of the impulsive model. The statistical reservoir is partitioned by assuming that each vibrational mode in the parent is adiabatically correlated to a particular degree of freedom in the products, e.g., parent torsions evolve exclusively into fragment rotation. The parent vibrational distribution is calculated using a harmonic density of states approximation. The average fragment vibrational, rotational, and translational energies from each reservoir, which separately conserve linear momentum, angular momentum, and total energy, are combined to give the final energies reported in Table 2. Unfortunately, the exit barrier height for CN elimination in acetyl cyanide has not been determined. We have, therefore, decided to treat this quantity as an adjustable parameter in our BIM calculations in order to estimate its value. We find that an exit barrier height of 24 kJ/mol reproduces the average experimental translational energy. The model also gives reasonable agreement with the majority of the experimental data except for the CN vibrational energy, which is overestimated. This suggests that the dissociation mechanism in acetyl cyanide is similar to that of other carbonyl compounds. The 24 kJ/mol exit barrier, presumably on the $^{1,3}(n,\pi^*)$ surface reached by internal conversion, is less than half that depicted in Figure 2, based on analogy with acetone and acetic acid. Since the exit barrier height for the CH_3 elimination channel is not known, it is uncertain whether the smaller barrier alone can explain the preference for primary CN elimination.

The average CH_3CO internal energy, calculated using the measured average CN vibrational, rotational, and translational energy, exceeds its 71 kJ/mol dissociation barrier.[14,50] This result suggests that the majority of the nascent CH_3CO fragments are unstable with respect to further fragmentation, an observation made previously by Horwitz *et al.*[19] We can quantify the fraction of the acetyl radicals which undergo secondary dissociation by considering the state-dependent CN translational energy distributions. From conservation of the energy it is possible to determine the internal energy distribution of CH_3CO fragments formed in coincidence with each given CN quantum state. Figure 8 shows the CH_3CO internal energy distributions corresponding to typical CN fragments in $v = 0$, 1, and 2. The shaded region of each plot indicates nascent acetyl radicals formed with insufficient energy to dissociate. Integrating the shaded region of each normalized distribution, weighted by the experimental vibrational distribution, yields the fraction of stable CH_3CO resulting from primary CN elimination. From this analysis we have determined a value of 0.007, which is consistent with the absence of CH_3CO^+ signal in the PTS experiment.

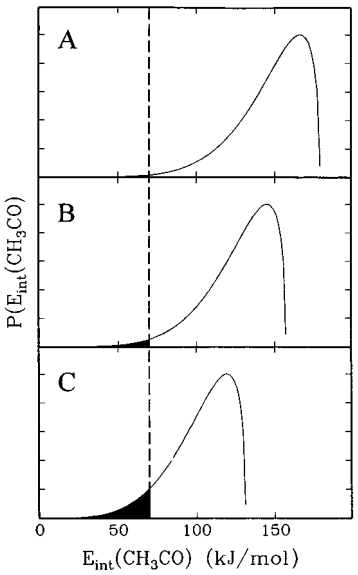

Figure 8. Predicted CH_3CO internal energy distributions calculated from the translational energy of selected CN fragments in (A) $v = 0$, $N = 24$, (B) $v = 1$, $N = 21$, and (C) $v = 2$, $N = 22$. The dashed lines indicates the threshold to CH_3CO dissociation and the shaded regions represent those CH_3CO fragments which do not have sufficient internal energy to dissociate.

V. Concluding Remarks

The complementary results obtained from the FM Doppler profiles, the CN quantum yield, and PTS measurements together produce a detailed view of the asymmetrical three-body dissociation of acetyl cyanide. The selective initial breaking of the C−CN bond is surprising, since it is not a direct excitation of a localized repulsive state, and it avoids a lower energy channel. Modeling of the CN energy distribution was most successful with a relatively low exit barrier of 24 kJ/mol for CN elimination, compared to other excited-state α-cleavage reactions in carbonyl compounds. If combined with an unusually large barrier to CH_3 elimination in the excited state, this could explain the preferential cleavage of the stronger bond. Further ab initio calculations on the $^{1,3}(n,\pi^*)$ excited-state potential energy surfaces would be helpful to investigate this possibility.

Acknowledgment. We thank Dr. Richard Holroyd for providing us with the UV spectrum shown in Figure 1 and Prof. Joseph Francisco for sharing prepublication work on the OCCN radical. The authors have benefited greatly from discussions with Prof. Joyce Guest. The PTS experiments were performed in the laboratory of Prof. J. R. Huber, whose support and interest are gratefully acknowledged. The remainder of work was performed at Brookhaven National Laboratory under Contract No. DE-AC02-76CH00016 with the U.S. Department of Energy and supported by its Division of Chemical Sciences, Office of Basic Energy Sciences.

References and Notes

(1) North, S. W.; Blank, D. A.; Gezelter, J. D.; Longfellow, C. A.; Lee, Y. T. *J. Chem. Phys.* **1995**, *102*, 4447.

(2) Hall, G. E.; Vanden Bout, D.; Sears, T. J. *J. Chem. Phys.* **1991**, *94*, 4182.
(3) Trentelman, K. A.; Kable, S. H.; Moss, D. B.; Houston, P. L. *J. Chem. Phys.* **1989**, *91*, 7498.
(4) Donaldson, D. J.; Leone, S. R. *J. Chem. Phys.* **1986**, *85*, 817. Donaldson, D. J.; Leone, S. R. *J. Phys. Chem.* **1987**, *91*, 3128. Woodbridge, E. L.; Fletcher, T. R.; Leone, S. R. *J. Phys. Chem.* **1988**, *92*, 5387.
(5) Gaines, G. A.; Donaldson, D. J.; Strickler, S. J.; Vaida, V. *J. Phys. Chem.* **1988**, *92*, 2762. Donaldson, D. J.; Gaines, G. A., Vaida, V. *J. Phys. Chem.* **1988**, *92*, 2766.
(6) Waits, L. D.; Horwitz, R. J.; Guest, J. A. *Chem. Phys.* **1991**, *155*, 149.
(7) At sufficiently short wavelengths in the vacuum ultraviolet the dissociation mechanism is substantially different, involving direct excitation to a repulsive $^1(n,\sigma^*)$ state: Kim, S. K.; Pedersen, S.; Zewail, A. H. *J. Chem. Phys.* **1995**, *103*, 477.
(8) Calvert, J. G.; Pitts, J. N. *Photochemistry*; Wiley: New York, 1966; pp 394−405.
(9) Reinsch, M.; Klessinger, M. *J. Phys. Org. Chem.* **1990**, *3*, 81.
(10) Person, M. D.; Kash, P. W.; Butler, L. J. *J. Phys. Chem.* **1992**, *96*, 2021. Person, M. D.; Kash, P. W.; Butler, L. J. *J. Chem. Phys.* **1992**, *97*, 355.
(11) Deshmukh, S.; Hess, W. P. *J. Chem. Phys.* **1994**, *100*, 6429. Deshmukh, S.; Myers, J. D.; Xantheas, S. S.; Hess, W. P. *J. Phys. Chem.* **1994**, *98*, 12535.
(12) North, S.; Blank, D. A.; Lee, Y. T. *Chem. Phys. Lett.* **1994**, *224*, 38.
(13) Sumathi, R.; Chandra, A. K. *J. Chem. Phys.* **1993**, *99*, 6531; *Chem. Phys.* **1994**, *181*, 73.
(14) Arunan, E. *J. Phys. Chem. A.* **1997**, *101*, 4838.
(15) Lane, I. C.; Meehan, R.; Powis, I. *J. Phys. Chem.* **1995**, *99*, 12371.
(16) North, S. W. Ph.D. Thesis, University of California, Berkeley, California, 1995.
(17) Kroger, P. M.; Riley, S. J. *J. Chem. Phys.* **1977**, *67*, 4483.
(18) Hunnicutt, S. S.; Waits, L. D.; Guest, J. A. *J. Phys. Chem.* **1989**, *93*, 5188. Hunnicutt, S. S.; Waits, L. D.; Guest, J. A. *J. Phys. Chem.* **1991**, *95*, 562. Peterman, D. R.; Daniel, R. G.; Horwitz, R. J.; Guest, J. A. *Chem. Phys. Lett.* **1995**, *236*, 564.
(19) Horwitz, R. J.; Francisco, J. S.; Guest, J. A. *J. Phys. Chem.* **1997**, *101*, 1231.
(20) Francisco, J. S.; Liu, R. *J. Chem. Phys.* **1997**, *107*, 3840.
(21) North, S. W.; Hall, G. E. *Chem. Phys. Lett.* **1996**, *263*, 148.
(22) North, S. W.; Hall, G. E. *J. Chem. Phys.* **1997**, *106*, 60.
(23) Bloch, J. C.; Field, R. W.; Hall, G. E.; Sears, T. J. *J. Chem. Phys.* **1994**, *101*, 1717.
(24) North, S. W.; Zheng, X. S.; Fei, R.; Hall, G. E. *J. Chem. Phys.* **1996**, *104*, 2129.
(25) Hall, G. E.; Wu, M. *J. Phys. Chem.* **1993**, *97*, 10911.
(26) Felder, P. *J. Chem. Phys.* **1990**, *143*, 141.
(27) Sparks, R. K.; Shobatake, K.; Carlson, L. R.; Lee, Y. T. *J. Chem. Phys.* **1981**, *75*, 3838.
(28) Nicholls, R. W. *J. Res. N.B.S.* **1964**, *68*, 75.
(29) Earls, L. T. *Phys. Rev.* **1935**, *48*, 423.
(30) Dixon, R. N. *J. Chem. Phys.* **1986**, *85*, 1866.
(31) Gericke, K.-H.; Klee, S.; Comes, F. J.; Dixon, R. N. *J. Chem. Phys.* **1986**, *85*, 4463.
(32) Ticktin, A.; Huber, J. R. *Chem. Phys. Lett.* **1989**, *156*, 372.
(33) Taatjes, C. A.; Cline, J. I.; Leone, S. R. *J. Chem. Phys.* **1990**, *93*, 6554.
(34) Dubs, M.; Brühlmann, U.; Huber, J. R. *J. Chem. Phys.* **1986**, *84*, 3106.
(35) August, J.; Brouard, M.; Simons, J. P. *J. Chem. Soc., Faraday Trans. 2* **1988**, *84*, 587.
(36) Schwartz-Levi, D.; Rosenwaks, S. *J. Chem. Phys.* **1988**, *88*, 6922.
(37) Press, W. H.; Flannery, B. P.; Teukolsky, S. A.; Vetterling, W. T. *Numerical Recipes*; Cambridge University Press: Cambridge, UK, 1986; p 402.
(38) Gordon, R. J.; Hall, G. E. *Adv. Chem. Phys.* **1996**, *96*, 1.
(39) Rudolph, R. N.; Hall, G. E.; Sears, T. J. *J. Chem. Phys.* **1996**, *105*, 7889.
(40) Eres, D.; Gurnick, M.; McDonald, J. D. *J. Chem. Phys.* **1984**, *81*, 5552. Huang, Y. Ph.D. Thesis, Howard University, Washington, DC, 1993.
(41) Furlan, A.; Scheld, H. A.; Huber, J. R. *Chem. Phys. Lett.*, in press.
(42) Assuming that each α-bond cleavage involves a similar 56 kJ/mol exit barrier, RRKM calculations using the vibrational frequencies given in ref 20 predict a 100:1 preference for the CH_3 + OCCN channel if the dissociation occurs on the $^1(n,\pi^*)$ excited state.
(43) Zamir, E.; Levine, R. D. *Chem. Phys.* **1980**, *52*, 25. Muckerman, J. T., unpublished results.
(44) Klippenstein, S. J.; Cline, J. I. *J. Chem. Phys.* **1995**, *103*, 5451.
(45) North, S. W.; Hall, G. E. *J. Chem. Phys.* **1996**, *104*, 1864.
(46) Uberna, R.; Hinchliffe, R. D.; Cline, J. I. *J. Chem. Phys.* **1996**, *105*, 9847.
(47) Busch, G. E.; Wilson, K. R. *J. Chem. Phys.* **1972**, *56*, 3639. Tuck, A. F. *J. Chem. Soc., Faraday Trans.* **1977**, *73*, 689.
(48) Fairbrother, D. H.; Dickens, K. A.; Stair, P. C.; Weitz, E. *Chem. Phys. Lett.* **1995**, *246*, 513.
(49) Osborn, D. L.; Choi, H.; Mordaunt, D. H.; Bise, R. T.; Neumark, D. M. *J. Chem. Phys.* **1997**, *106*, 3049.
(50) Watkins, K. W.; Word, W. *Int. J. Chem. Kinet.* **1974**, *6*, 855.